Progress In Electromagnetics Research C, Vol. 80, 89–101, 2018

Metal-covered Handset with LTE MIMO, Wi-Fi MIMO, and GPS Antennas

Joni Kurvinen[1, *], Anu Lehtovuori[1], Jianchun Mai[2], Chao Wang[2], and Ville Viikari[1]

Abstract—Current phones include more metal than earlier, which deteriorates the performance of antennas. This paper presents the first complete antenna set designed for a modern handset with a full metal back cover. 4G, Wi-Fi, and GPS antennas are integrated into the metallic side frame of the device in a realistic model. The designed antennas are either capacitive coupling elements with reactive loads or slot antennas. Fixed matching circuits are used to improve total efficiency. The passive implementation enables the use of carrier aggregation (CA) to increase the data rates, and includes also the multiple-input multiple-output (MIMO) operation for 4G and Wi-Fi. The designed antennas cover frequency bands 704–960 MHz, 1.56–1.61 GHz, 1.71–2.69 GHz, 2.4–2.484 GHz, and 5.15–5.875 GHz, producing in measurements a good agreement with simulation results.

1. INTRODUCTION

Modern smartphones have become the everyday tool used also in demanding conditions. Wireless networks have spread everywhere, so connection can be established in any environment. Therefore, mobility of people is not restricted by the performance of the devices anymore. Instead, mechanical strength is required from the device to protect itself and its subsystems from physical damage. Also, from industry-point-of-view, consumer products have to be visually appealing. A recent trend among phone manufacturers has been using metal covers in flagship models to improve both the robustness and aesthetics of the device. However, using highly conductive housing materials creates a challenge. Enclosing antennas with metallic structures prevents radiating and impedes establishing a communications link.

Problems caused by the increased amount of metal have been countered by new type of antennas that are integrated into the housing structure [1–7]. Previous studies have shown promising performance with different antenna configurations. The first solutions include only metallic side frame. Grounding the frame from few locations creates a dual-loop antenna [1, 2], which excites several resonant modes. Loop antennas generally have been a popular choice as presented in [3–5, 9]. Also monopoles integrated into the rim have been in use [6, 7, 10].

The next step from metal-rimmed phones is a metallic back cover. A larger volume of metal increases the size of the RF-ground, which restricts the antenna size and placement possibilities even more. To ensure good antenna performance, phone manufactures have cut slots into the back cover, as is seen in many commercial products, or proposed in, e.g., [11–17]. Slotless covers have been presented in [18, 19], but they have large openings in the side rim for the antennas.

Another challenge for antennas comes from the current network standards. Smartphones must be able to operate on several frequency bands. Bands are wide, and covering all of them requires many antennas. Utilizing multiple-input multiple-output (MIMO) communications and carrier aggregation

Received 23 August 2017, Accepted 24 November 2017, Scheduled 8 December 2017

* Corresponding author: Joni Kurvinen (joni.kurvinen@aalto.fi).

[1] Department of Electronics and Nanoengineering, School of Electrical Engineering, Aalto University, Espoo, AALTO FI-00076, Finland. [2] AAC Technologies Co., Ltd., Nanjing 210093, China.

(CA) techniques to achieve higher data rates also increases the number of antennas. In mobile devices, the space available for antennas is very limited due to the compact physical dimensions and maximized size of a touchscreen. Altogether, these practical aspects make it more difficult to achieve good performance. One promising approach in multiantenna design is to use the theory of characteristic modes [8].

This paper presents a multiband antenna system for a realistic smartphone with fully metallic back cover. Antennas cover LTE low band (LB, 704–960 MHz), LTE high band (HB, 1710–2690 MHz) and Wi-Fi (2.4 GHz, 5 GHz) bands with MIMO and CA capability. In addition, the design also supports GPS (1.575 GHz) operations. As far as we know, this is the first study presenting a complete antenna solution for a metal-covered handset. Although the designed antenna structures are well-known, the novelty here is the used antenna combination that fits inside a smartphone and provides decent performance. Figure 1 presents the main parts of the simulation model and the detail in the used model. Our design has fixed antenna structures and matching circuitries for all frequencies, slotless metallic back cover, metallic side frame, and realistic phone model with subsystems, which are generally not included in recent papers. Table 1 lists all antennas and their operational frequencies.

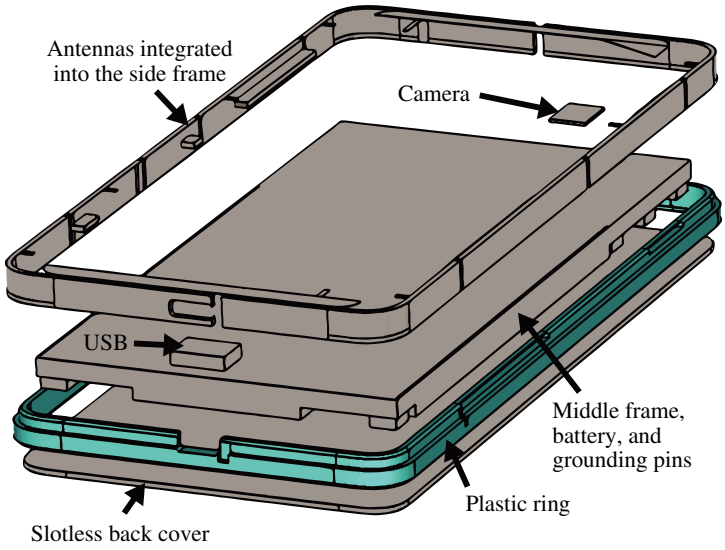

Figure 1. Exploded view of the simulation model.

Table 1. Operational frequencies of each antenna and their respective ports in the simulation model.

Antenna	Frequencies (MHz)	Port
Main LB	704–960	1
Main HB	1710–2690	8
Diversity HB	1710–2690	4
Diversity LB	704–960	5
Wi-Fi 1	2400–2484, 5150–5875	7
GPS & Wi-Fi 2	1560–1610, 2400–2484, 5150–5875	9

Operational principle of the design is introduced in Section 2. Section 3 presents the proposed antenna solutions in detail with impedance matching results. The efficiency results and MIMO performance from simulations and measurements are presented in Section 4. Some conclusions are given Section 5.

2. DESIGN FRAMEWORK AND PRINCIPLES

This study aims to design a realistic structure, and hence we use a very accurate simulation model from the beginning. The model includes also many realistic details such as battery, USB-port, and front camera, as shown in Figure 1. A plastic rim separates the back cover and side frame from each other. A large middle frame is in the center of the device modeling the touchscreen and other electronics of the phone, and it also acts as the RF-ground for the antennas together with the back cover. Similar realisticity of design model is earlier seen in [14, 15]. The size of the device is $151 \times 75.8 \times 7.63\,\text{mm}^3$, which is roughly the same as that of, e.g., iPhone 7 Plus or Samsung Galaxy S7 edge's. Ground clearance between the middle frame and the side frame is 2.5 mm in the sides, and 10.2 or 7.8 mm in the ends. The key property of the model is the slotless metallic back cover, seen in Figure 2(a).

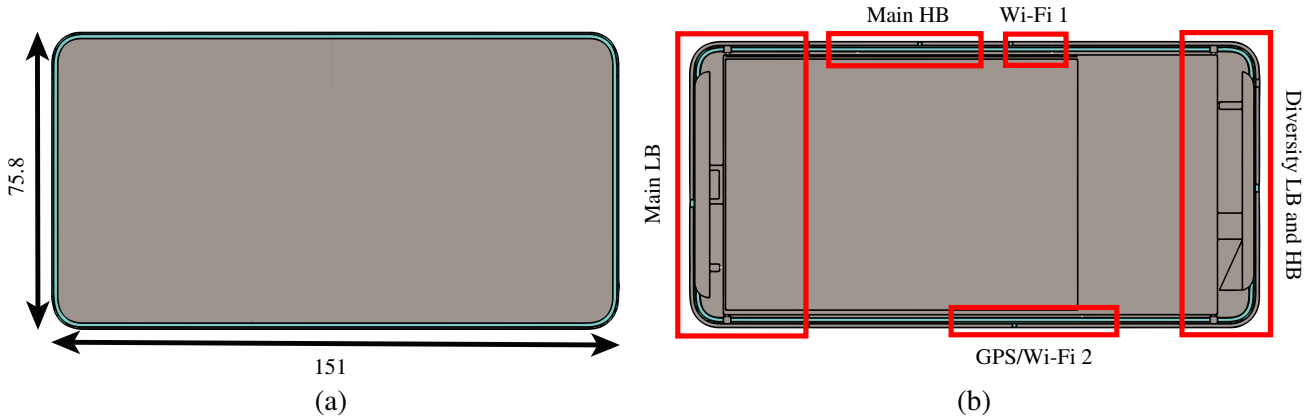

Figure 2. Simulation model showing the slotless back cover and physical dimensions in mm in (a), and the location of each individual antenna in (b). Maximum thickness of the device is 7.63 mm.

The proposed antennas are of Capacitive Coupling Element (CCE) type [20, 21], or slot antennas. CCEs are widely used at cellular frequencies due to their wide frequency band and robust performance. Slot antennas are appropriate for sides of the phone with only narrow 2.5 mm clearance for antennas [1, 3]. Each antenna has additional matching circuit to adjust the resonances to desired frequency bands and to enhance performance. Matching components in simulations are models of actual Murata inductors and capacitors (LQW18 and GQM18 series, respectively). Antenna structures are studied by conducting electromagnetic simulations in CST Microwave Studio [22]. Matching circuitry is created and optimized in Optenni Lab [23]. Table 1 lists all designed antennas and also their respective port numbers in the simulation model. Same port numbers are later used in this paper when presenting the performance of the antennas.

Since the simulation model consists of realistic shapes and details, the computing times of EM-simulations become very long. Therefore, antennas are designed and simulated in the first phase one by one to reduce simulation times. Low coupling between different frequencies allows this method, and all antenna elements and ports can be taken into account only in the last simulations when fine-tuning the dimensions of structures and matching component values.

Implementation of the antennas starts with the cellular antennas. One end of the device is reserved for the main antenna, and the other one for the diversity antenna. Figure 2(b) shows the final positions of the antennas. First, we design the low band of the main antenna since lower frequencies are the most challenging and require the largest physical size. Second, a solution for the main HB is added. The main antenna structure has been the basis of the diversity antenna for MIMO capability. The last antennas to include are the GPS and Wi-Fi antennas operating at higher frequencies. They are located at the long sides of the device. For improved performance in the final design, LB and HB of the main antenna are separated to individual configurations such that HB is placed to the side rim and LB utilizes the end completely. Matching networks for each element are adjusted continuously when structural changes are made.

The aesthetic properties expected from a real device have been in the guideline and a restricting factor in the design process. For example, the width of all cuts in the metal rim is 1 mm in the sides and 2 mm in the ends. In addition, the slots are located as symmetrically as possible around the device, to keep in mind the visual appearance of a possible end-product. The continuous metal rim is required to go around the device, which has determined the antenna structures.

2.1. Three-element Antennas in the Ends of the Phone

Main and diversity antennas are based on the closely located antenna elements [24] that couple strongly to each other and the ground plane, which improves impedance matching [24, 25]. However, mutual coupling between ports decreases efficiencies. The negative effects of large mutual coupling are countered with careful matching circuit design in the final solutions.

Matching circuit design is done by defining pass- and stop-bands for each port in Optenni Lab. This way the radiated power is maximized and mutual coupling reduced. Operational bandwidths of these antennas are improved with grounding inductances. Similar reactive loading is used, e.g., in [26, 27].

2.2. Slot Antennas on the Sides of the Phone

The antennas for higher frequencies are implemented as slot-type antennas on the sides of the phone. Figure 3 presents the basic principle of the slot antennas. The metal rim is grounded by connecting to the middle frame of the device. The slot is cut to the grounding metal, and also to the side rim. Slot antennas are applicable with very small clearance.

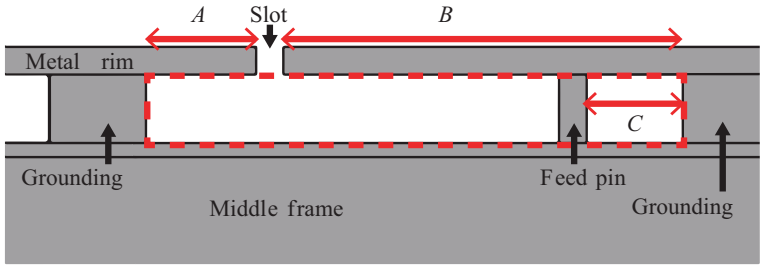

Figure 3. Principle of a slot antenna illustrated from the top of the phone.

The two branches (A and B) separated with a 1 mm cut in the metal rim are the main resonators of this design. The resonant frequencies can be tuned by changing the lengths of A and B. Basically, this means enlarging the clearance area (dashed area in Figure 3), so that the width and location of the slot with respect to the chassis remain the same.

For example, in the case of a Wi-Fi antenna, tuning the length A affects the 5 GHz band and length B the 2.4 GHz band. Generally, the longer one branch is, the lower its resonance frequency becomes. By adjusting the feed location, i.e., length C, the matching levels can be balanced.

3. PROPOSED ANTENNAS

Traditionally, mobile antennas are required to have -6 dB matching level. Nowadays, the design framework is more complex, as the clearances are smaller and industry sets strict constraints to the aesthetics. Thus, the same matching level is challenging to achieve [14, 15]. Therefore, we have focused on realizing moderate impedance matching at correct frequency bands, and maximizing the efficiencies, which are presented in Section 4. Next, the antenna structures are introduced in detail with impedance matching results.

3.1. Main Antenna

The LB and HB of the main antenna have been implemented as separate structures. Figure 4 shows the geometry of the LB antenna. The structure consists of two L-shaped parts in the side rim and

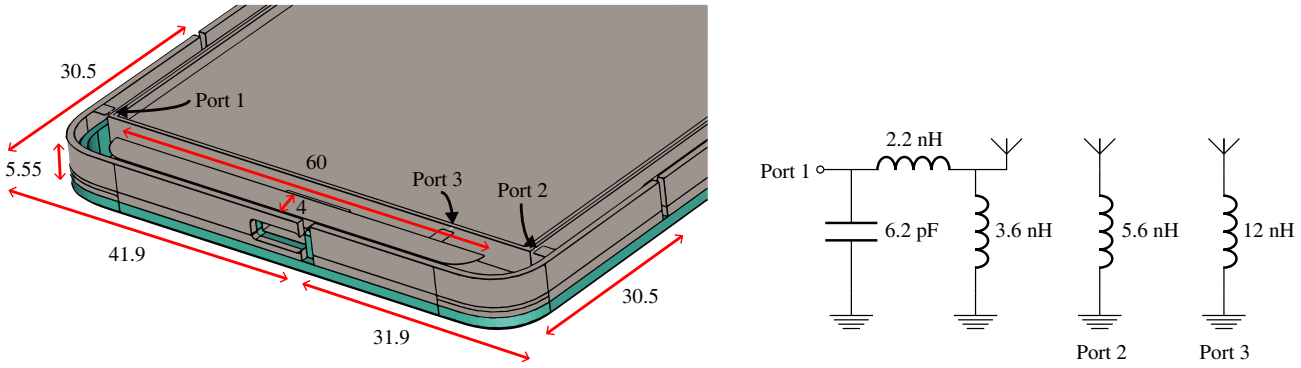

Figure 4. Configuration for main cellular antenna's low band operation. Port 1 is fed through a matching circuit shown on the right, and aperture matching elements in Ports 2 and 3 are grounded with inductances. All dimensions are in mm.

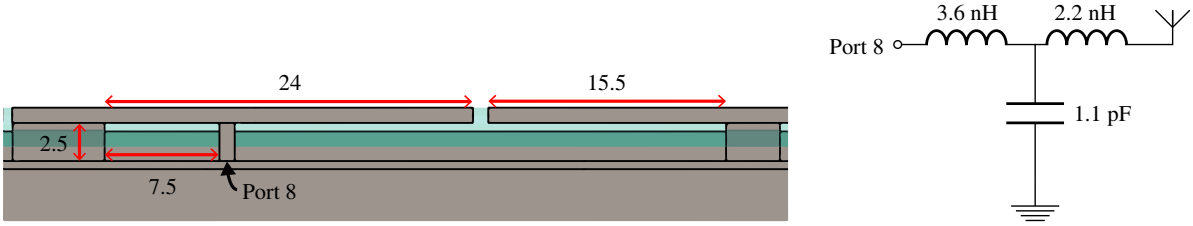

Figure 5. Main antenna configuration for high band operation from topside of the phone. The used matching circuit is seen on the right. All dimensions are in mm.

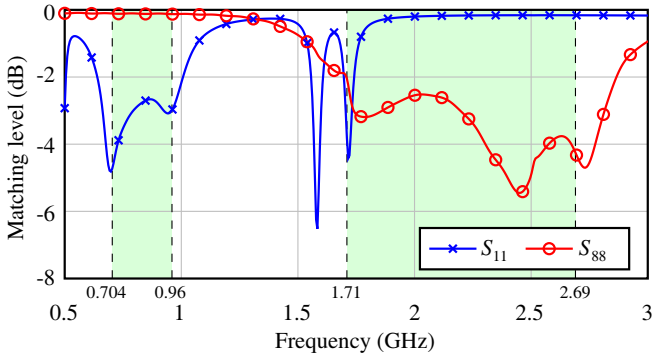

Figure 6. Matching levels for the main cellular antenna.

parasitic coupler on the front face of the phone. The feed is connected to larger L-shaped element (Port 1), and aperture matching elements are connected with grounding inductances to Ports 2 and 3. The dimensions of the elements are optimized together with circuit elements to achieve the desired operation.

In order to get more freedom to design, HB antenna is implemented with a slot antenna as shown in Figure 5. The metal rim around the phone is cut with 1 mm slot, and the rim is grounded to the middle frame from unnecessary areas from antenna point of view. This grounding also significantly improves the isolation between antennas.

Previously published designs use additional slots in the back cover [11–13] to improve the performance at remarkable way. Therefore, in this design maximizing efficiency has been the main design target, since the slotless cover makes achieving −6 dB matching level practically impossible. Figure 6 shows that the main antenna reaches mainly −3 dB matching level over both operational bands.

3.2. Diversity Antenna

The diversity antenna for MIMO communications is located at the opposite end of the phone other than the main antenna. This structure shown in Figure 7 has the same basic idea as the main LB antenna, but now both L-shaped elements are fed. With suitable matching circuits Port 4 covers HB while Port 5 operates the LB. The triangle at one end of the parasitic coupler connected to Port 6 is introduced to fine-tune the resonances and enhance the desired performance. The triangle makes the parasitic element behave longer electrically, which lowers the highest resonances from out-of-the-band frequencies to the correct range. Idea for this extension is based on [28], in which trapezoidal feeds are used to achieve wider operational band.

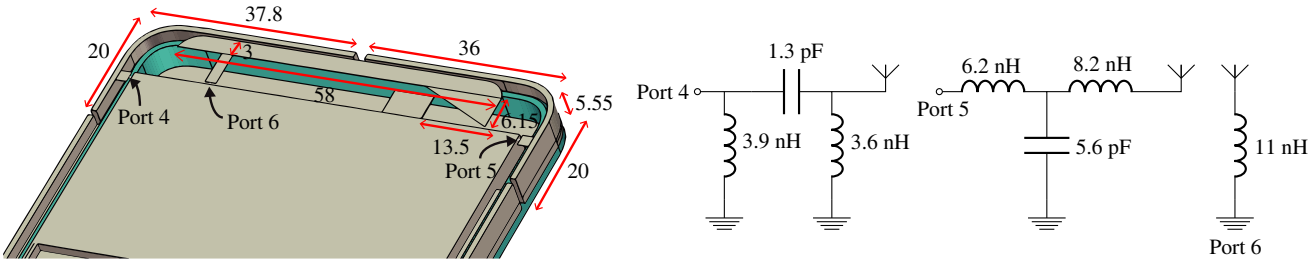

Figure 7. Geometry and matching circuitry for diversity cellular antenna. Port 4 is for LB and Port 5 for HB. Port 6 is for aperture matching. All dimensions are in mm.

Figure 8 shows the matching levels of the diversity antenna. Compared to the main antenna, the impedance matching level is about 1 dB lower, because due to the structural non-symmetries (camera, USB, and ground clearance) the ends of the phone are different, and hence the volume available for the antennas is different. Moreover, in the diversity antenna, LB and HB are realized with the same structure, which further restricts the usable volume. The structural differences between the two ends do not allow the same separation of LB and HB to used also in the diversity antenna. Also the side parts of the L-shaped elements are longer in the main antenna, which partly explains the different performance.

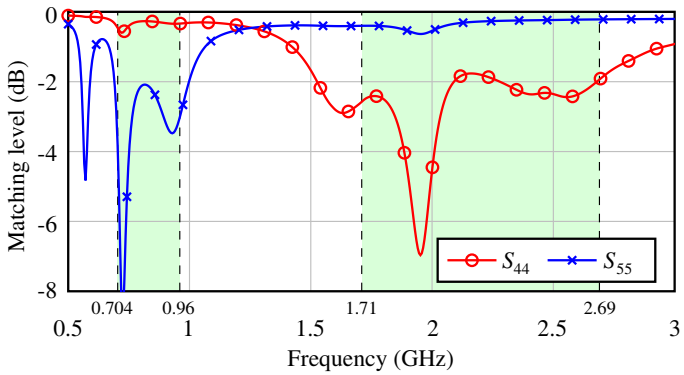

Figure 8. Matching levels for the diversity cellular antenna.

3.3. GPS and Wi-Fi Antennas

Nowadays mobile phones have to support GPS and Wi-Fi. Antennas for this are located on the long sides of the device, and are similar slot antennas as the main cellular HB antenna. Detailed dimensions of Wi-Fi 1 and GPS/Wi-Fi 2 antennas are shown in Figure 9. Both of the antennas support Wi-Fi at 2.4 GHz and 5 GHz bands, and one of the two operates also on GPS band at 1.575 GHz as seen in Figure 10.

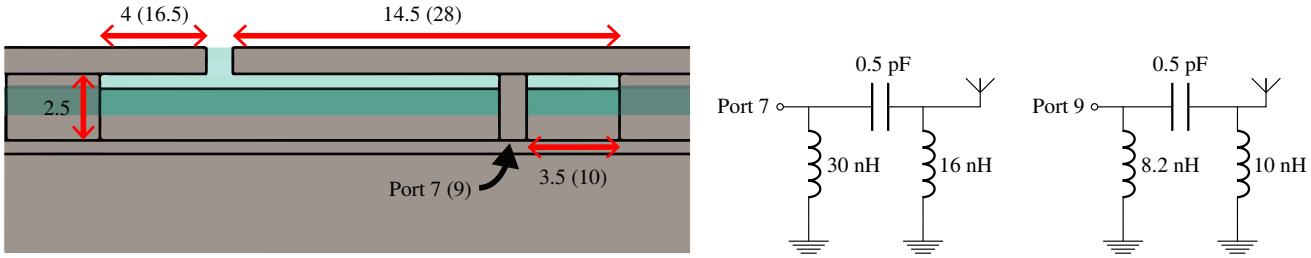

Figure 9. Antenna configuration from the top of the phone for Wi-Fi 1 antenna in Port 7. The dimensions in the parentheses are for GPS/Wi-Fi 2 antenna in Port 9. Matching networks for both antennas are seen on the right. All dimensions are in mm.

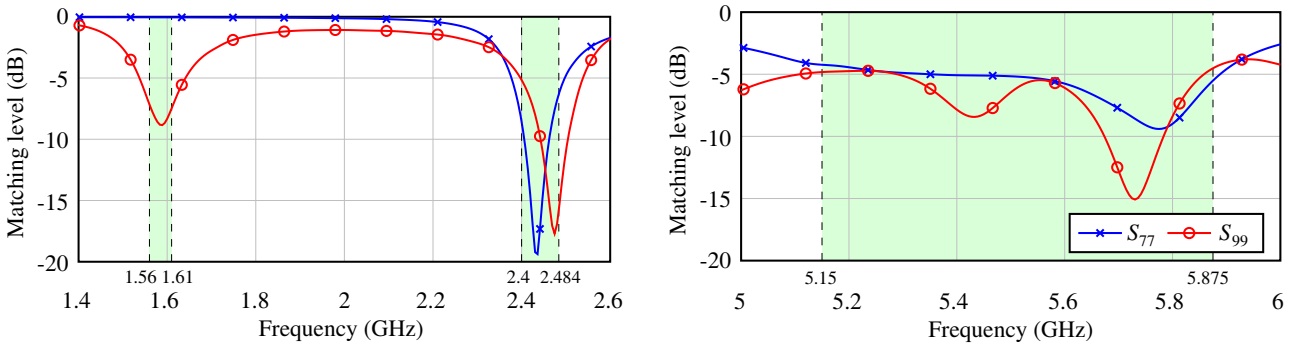

Figure 10. Matching levels for GPS and Wi-Fi antennas.

Figure 10 shows the matching levels of Wi-Fi and GPS antennas. In contrast to cellular antennas, these obtain at least −5 dB matching over the desired bands.

3.4. Antenna Isolation

Especially at the low band achieving good antenna isolation is difficult as the ground plane acts as the main radiator for two antennas. Figure 11 shows the simulated coupling at the cellular frequencies. Generally, the four antenna ports are well-isolated as the coupling levels are −15 dB or better. As expected, due to the common antenna structure, the largest coupling S_{54} is between diversity LB and HB. Still, they are well-isolated as the mutual coupling is below −12 dB over the whole frequency bands.

Figure 12 shows the couplings at the GPS and Wi-Fi frequencies. Clearly, the cellular antennas

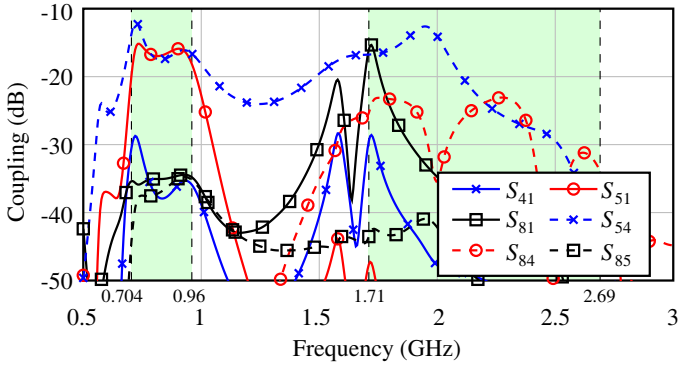

Figure 11. Coupling at cellular frequency bands.

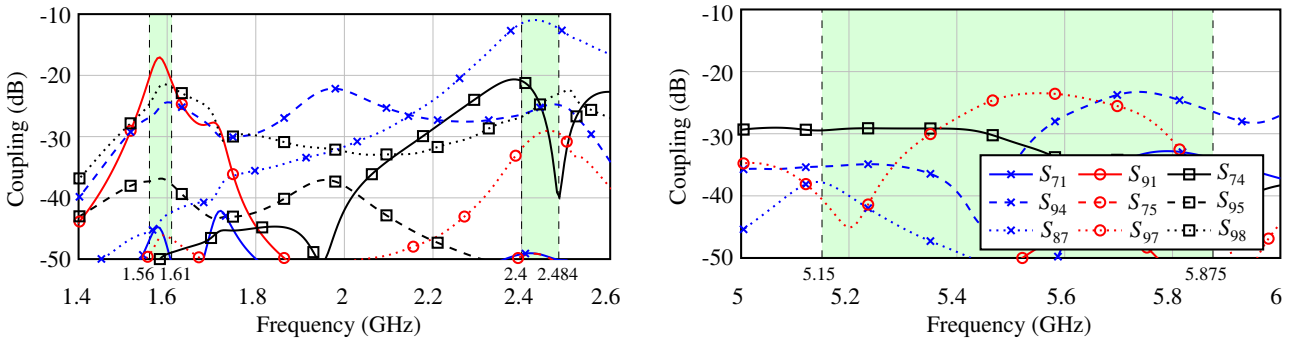

Figure 12. Antenna coupling between cellular and Wi-Fi antennas.

are well-isolated in these bands as the operational frequencies are different. Since the distance between Main HB and Wi-Fi 1 antennas is physically and electrically very small (see Figure 2(b)), the coupling between the two antennas (S_{87}) in their shared operational band is larger than in other cases, peaking at -11 dB. Although the antenna isolations are generally already on very good levels, they could possibly be improved further by embedding metamaterial structures [29, 30].

4. ANTENNA PERFORMANCE

The main target of this study is to achieve decent total efficiencies, at least 30%, in simulations for each individual antenna. In addition, MIMO and CA capabilities are analyzed with envelope correlation coefficient (ECC). To confirm the obtained simulation results, a prototype of the structure is manufactured and then measured. The middle frame (see Figure 1) and parts connected to it, including the grounded side antennas, are made of solid brass by milling. The back cover is made from aluminum. Top 0.8 mm of the middle frame is replaced with an FR-4 printed circuit board (PCB), on which the matching circuits are realized. Plastic ring is made of injection moldable plastic PREPERM® L335 [31], whose dielectric constant is 3.35 and loss tangent 0.0005. The constructed prototype and measurement setup is shown in Figure 13.

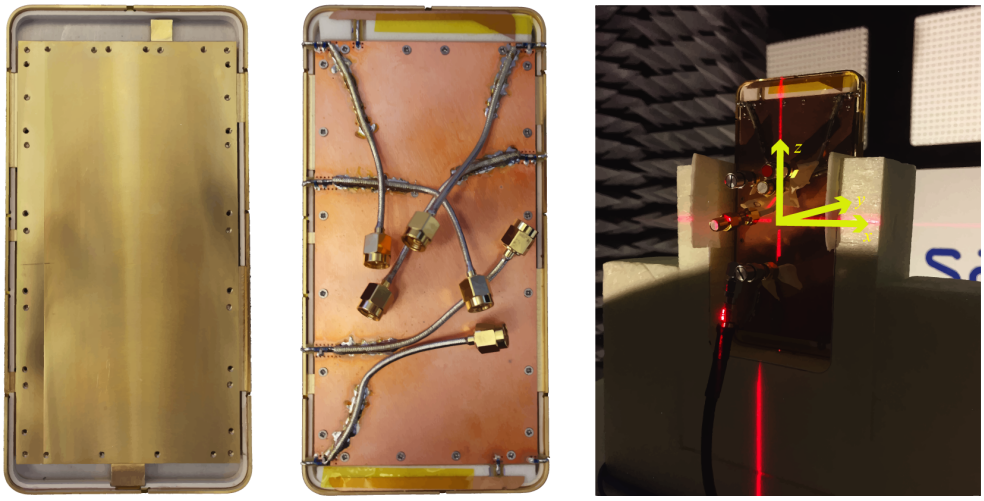

Figure 13. Constructed prototype (a) without and (b) with the PCB and front face elements. Drilled holes seen in (a) are used for attaching the back cover and PCB to the middle frame. (c) The measurement setup in Satimo StarGate with the used coordinate system.

4.1. Radiation Performance

Current transmitters tolerate a significant amount of impedance mismatch, and hence the antenna performance is mainly dominated by the radiation efficiency. Due to large amounts of metal in this structure, the matching levels of especially cellular antennas remain rather modest. Hereby the overall performance is analyzed by total antenna efficiency. Figure 14 shows simulated total efficiencies for all designed antennas, compared with measured results.

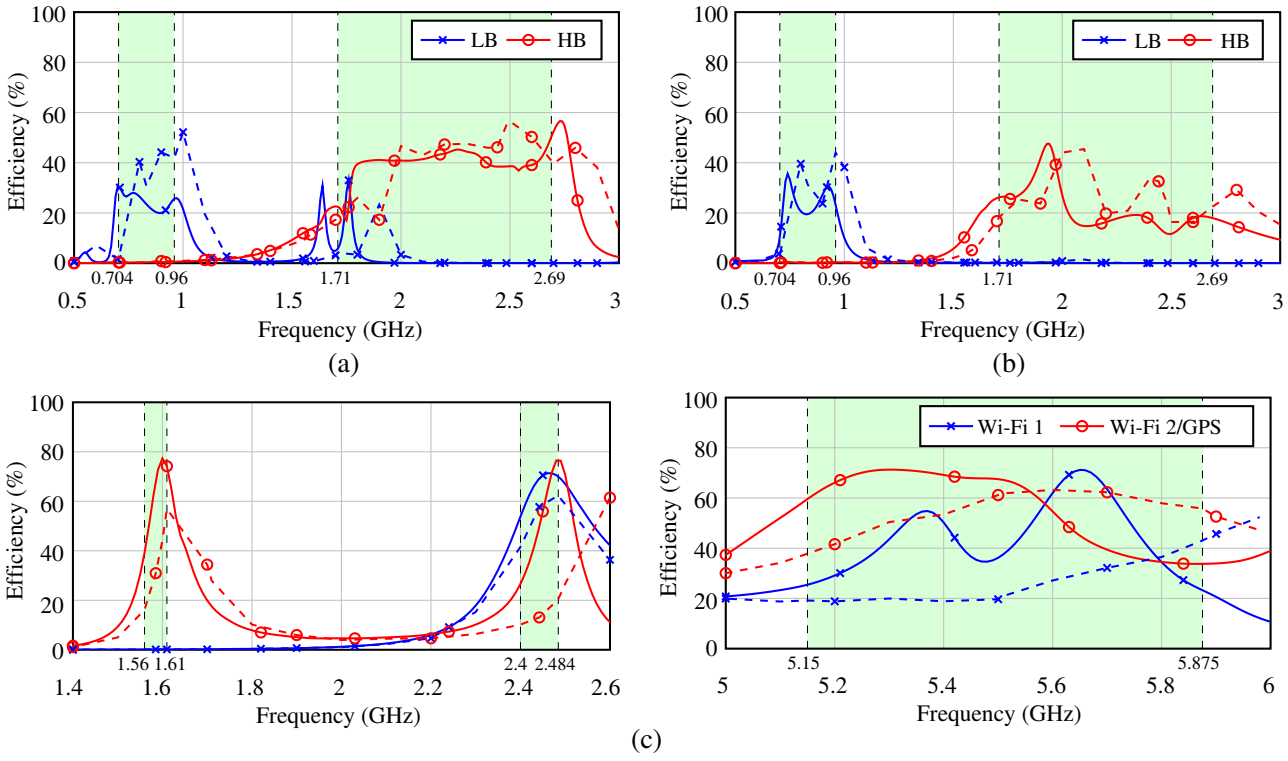

Figure 14. Total efficiencies for (a) main, (b) diversity, and (c) GPS and Wi-Fi antennas. Solid lines are simulated and dashed lines measured efficiencies.

For the main antenna, simulated total efficiencies are 30–40%, as shown in Figure 14(a). Diversity antenna with slightly different design performs with 20–40% efficiency (Figure 14(b)). These simulated results are in line with impedance matching results.

In recent publications, cellular antennas in metal-covered phones typically reach efficiencies over 40% [11–13, 19]. Although the simulated efficiencies are lower than those values, the target level of 30% for total efficiency is mainly achieved. However, our model is more realistic and has the slotless back cover, which is not seen in previous papers. Therefore, it is more convenient to compare our results with [14, 15], which present solutions of similar realisticity.

Our measured efficiencies confirm the simulations very well. Moreover, LB of the main antenna is even better than in simulations, peaking at 50%. Main HB and diversity antennas are very similar with simulations with efficiencies ranging between 20–40%. A small frequency shift is observed as all bands appear at slightly higher frequencies in measurements than in simulations. In [14, 15], generally the same measured efficiency levels are reached, but with tunable solutions.

Wi-Fi and GPS antennas perform very well in the simulations, as Figure 14(c) shows. Both antennas reach at least 40% and up to 80% total efficiency. In measurements, we notice similar but stronger frequency shift to the higher frequencies as with cellular antennas. Especially Wi-Fi 2 antenna is shifted up at 2.4 GHz being completely out of the band. By adjusting component values, or including more circuit elements to the matching network, the resonance can be moved to the desired band without

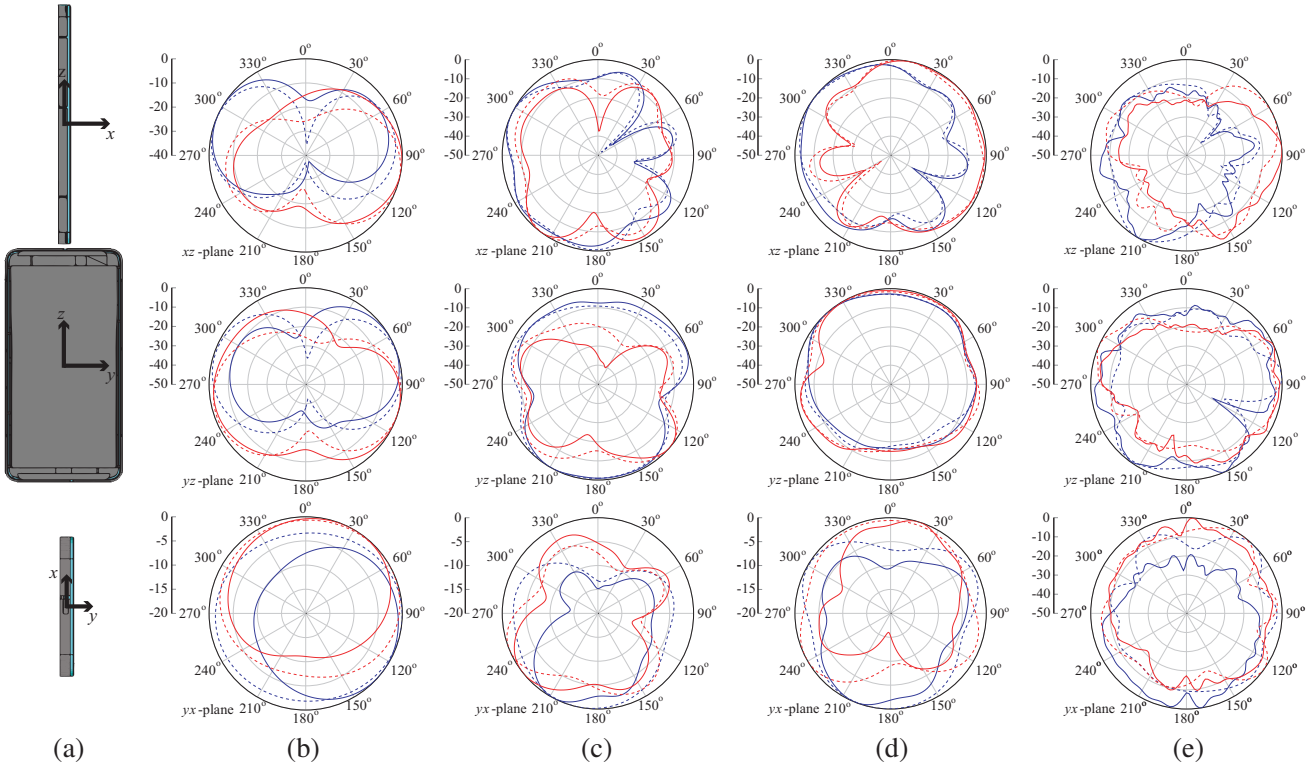

Figure 15. Cutting planes (a) and radiation patterns of cellular antennas at (b) 830 MHz, (c) 2300 MHz, and Wi-Fi antennas at (d) 2400 MHz, and (e) 5500 MHz. Blue curves correspond to the main or Wi-Fi 1 antenna, and red to the diversity or Wi-Fi 2 antenna. Solid lines are the measured fields and dashed the simulated. Unit is dB.

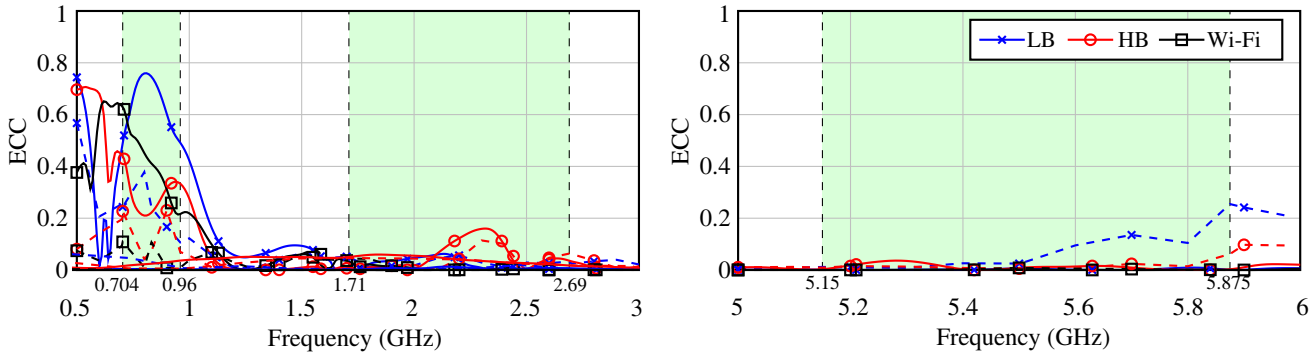

Figure 16. Simulated (solid lines) and measured (dashed lines) envelope correlation coefficients for all MIMO antennas.

hurting the peak efficiencies. Generally, the measured GPS and Wi-Fi efficiencies are 40–60%, and are in the same range as in [13, 18].

Measured and simulated normalized radiation patterns are shown in Figure 15. Figure 15(a) illustrates the orientation of the phone in each plane. In xz- and yx-planes, the metal cover is in the right side of the device. The measured patterns match the simulations very well. In most cases, the antennas radiate nicely in all directions, although some strong nulls are observed.

4.2. MIMO/CA Capability

To analyze the MIMO/CA performance of the designed antennas, Envelope Correlation Coefficients (ECC) [32] are calculated from far-field results for each MIMO antenna pair. Figure 16 shows simulated and measured ECCs in each case. The correlation in the high band and Wi-Fi frequencies is minimal. As can be expected, ECC is the highest at the low band. This is due to the coupling of antennas to the chassis. Similarly, the strongest correlation of HB and Wi-Fi antennas appears below 1 GHz, even though the antennas do not operate at that frequency range.

The correlations calculated from the measured fields are in good agreement with simulations, but at clearly better levels. Generally, ECC is required to be below 0.5 for the antennas to be suitable for MIMO and CA operations. The measured peak correlation of LB antennas is now 0.4, which satisfies the general requirement for MIMO. In HB and Wi-Fi bands, the correlations are even less, staying at below 0.2. Due to the fixed antenna structures and good ECC, the designed antennas can be used in CA applications as well.

4.3. State-of-the-Art Comparison

Table 2 presents a comparison between the proposed design and other previously published antenna systems for metal-covered handsets. This comparison highlights the fact that our design is the first MIMO-capable, complete antenna system for metal-covered handsets. Most of other designs do not have any MIMO, and many operate on fewer frequencies. Moreover, the LTE LB starts from 700 MHz in our design, which is not the case with many other systems. In addition, we achieve similar performance with fixed antenna and matching structure, while some require tunable solutions.

Table 2. Comparison of proposed design and previously published antennas in metal-covered handsets. *LB from 746 MHz upwards, ⋆LB from 850 MHz upwards, §HB up to 2200 MHz, #only 2.4 GHz Wi-Fi, ♣includes only metal rim, ♠simulated value.

Ref.	Operational bands	Measured efficiency	MIMO capability	Measured ECC	Antenna implementation
This work	**LTE LB & HB, GPS, Wi-Fi**	**20–60%**	**LB, HB, Wi-Fi**	**LB $<$ 0.4, HB $<$ 0.1**	**Fixed**
[11]	LTE LB* & HB	28–72%	LB, HB	$<$ 0.19	Fixed
[13]	LTE LB⋆ & HB§, GPS, Wi-Fi#	40–65%	-	-	Fixed
[14]	LTE LB & HB	20–55%	-	-	Tunable
[15]	LTE LB & HB	20–50%	-	-	Tunable
[17]	LTE LB & HB	40–70%	-	-	Fixed
[18]	GPS, Wi-Fi	40–70%	-	-	Fixed
[2]♣	LTE LB & HB	45–90%♠	HB	$<$ 0.5♠	Fixed
[8]♣	LTE LB	25–40%	LB⋆	$<$ 0.1	Fixed
[9]♣	LTE LB & HB	45–90%	LB, HB	LB $<$ 0.18, HB $<$ 0.1	Tunable

5. CONCLUSIONS

This paper presents a realistic metal-covered handset design with LTE, GPS, and Wi-Fi antennas including MIMO operation. The proposed structure is the first complete antenna system for fully metal-covered smartphone. In spite of the huge effect of a continuous metal cover, the acceptable efficiency performance is achieved without tunable circuit components. Especially, the design takes into account many essential components of the real device. Also, the design is capable of carrier aggregation in the cellular bands due to the fixed antenna and matching structures.

ACKNOWLEDGMENT

This work was supported by AAC Technologies Co., Ltd. The authors would like to thank Mr. Eino Kahra for his professional help in manufacturing the prototypes, and Dr. Mikko Keskilammi for antenna measurements on very tight schedule.

REFERENCES

1. Ban, Y. L., Y. F. Qiang, Z. Chen, K. Kang, and J. H. Guo, "A dual-loop antenna design for hepta-band WWAN/LTE metal-rimmed smartphone applications," *IEEE Trans. Antennas Propag.*, Vol. 63, No. 1, 48–58, Jan. 2015.
2. Stanley, M., Y. Huang, H. Wang, S. S. Alja'afreh, Q. Xu, and L. Xing, "LTE MIMO antenna using unbroken metallic rim and non resonant CCE element," *Proc. 10th Eur. Conf. on Antennas Propag. (EuCAP)*, 1–4, Davos, Switzerland, Apr. 2016.
3. Hsu, C. K. and S. J. Chung, "Compact multiband antenna for handsets with a conducting edge," *IEEE Trans. Antennas Propag.*, Vol. 63, No. 11, 5102–5107, Nov. 2015.
4. Ban, Y. L., Y. F. Qiang, G. Wu, H. Wang, and K. L. Wong, "Reconfigurable narrow-frame antenna for LTE/WWAN metal-rimmed smartphone applications," *IET Microw. Antennas Propag.*, Vol. 10, No. 10, 1092–1100, Jul. 2016.
5. Lian, J. W., Y. L. Ban, Y. L. Yang, L. W. Zhang, C. Y. D. Sim, and K. Kang, "Hybrid multi-mode narrow-frame antenna for WWAN/LTE metal-rimmed smartphone applications," *IEEE Access*, Vol. 4, 3991–3998, Jul. 2016.
6. Lee, D., W. C. Choi, J. Ahn, and Y. J. Yoon, "A simple monopole antenna for hepta-band LTE/WWAN metal-framed mobile phone," *Proc. Int. Symp. Antennas Propag. (ISAP)*, 1–3, Hobart, Australia, Apr. 2015.
7. Chen, H. and A. Zhao, "LTE antenna design for mobile phone with metal frame," *IEEE Antennas Wireless Propag. Lett.*, Vol. 15, 1462–1465, Dec. 2015.
8. Qu, L., H. Lee, H. Shin, M. G. Kim, and H. Kim, "MIMO antennas using controlled orthogonal characteristic modes by metal rims," *IET Microw. Antennas Propag.*, Vol. 11, No. 7, 1009–1015, Jun. 2017.
9. Stanley, M., Y. Huang, H. Wang, H. Zhou, Z. Tian, and Q. Xu, "A novel reconfigurable metal rim integrated open slot antenna for octa-band smartphone applications," *IEEE Trans. Antennas Propag.*, Vol. 65, No. 7, 3352–3363, Jul. 2017.
10. Yang, Y., Z. Zhao, W. Yang, Z. Nie, and Q. H. Liu, "Compact multimode monopole antenna for metal-rimmed mobile phones," *IEEE Trans. Antennas Propag.*, Vol. 65, No. 5, 2297–2304, May 2017.
11. Son, T. and Y. Jo, "Wideband mobile MIMO antenna for the metal cover phone," *Proc. IEEE Region 10 Conf. (TENCON)*, 1–3, Macao, China, Nov. 2015.
12. Wu, C. Y., Y. L. Kuo, and K. C. Lin, "Low-profile tunable WWAN antenna for whole-metal-covered mobile phone applications," *Proc. Int. Symp. Antennas Propag. (ISAP)*, 275–276, Kaohsiung, Taiwan, Dec. 2014.
13. Zhong, J., R. M. Edwards, L. Ma, and X.-W. Sun, "Multiband slot antennas for metal back cover mobile handsets," *Progress In Electromagnetics Research Letters*, Vol. 39, 115–126, Apr. 2013
14. Tan, Y. C. M., N. G. G. Hong, and Y. S. R. Tay, "Tuning of LTE main antenna using flexible tunable LC resonant circuitry," *Proc. 11th Eur. Conf. Antennas Propag. (EuCAP)*, 3082–3085, Paris, France, Mar. 2017.
15. Tan, Y. C. M., N. G. G. Hong, and Y. S. R. Tay, "A tunable LTE main antenna solution for metallic cover mobile phone," *Proc. 11th Eur. Conf. Antennas Propag. (EuCAP)*, 2969–2972, Paris, France, Mar. 2017.
16. Kumar, P. and J. Thakur, "Antenna for metal body mobile devices," *Proc. IEEE Indian Antenna Week (IAW)*, 75–77, Madurai, India, Jun. 2016.

17. Chang, C. K., W. J. Liao, and C. C. Tsai, "Metal body-integrated open-end slot-antenna designs for handset LTE uses," *IEEE Trans. Antennas Propag.*, Vol. 64, No. 12, 5436–5440, Dec. 2016.
18. Wu, Z., H. Wang., P. Chen, W. Shen, and G. Yang, "A compact GPS/WLAN antenna design for mobile terminal with full metal housing," *Progress In Electromagnetics Research C*, Vol. 64, 169–177, Jun. 2016.
19. Chen, P., P. Wang, Y. Yu, and G. Yang, "A compact LTE antenna design for mobile device with full metal housing," *Proc. Int. Workshop Antenna Technology (iWAT)*, 23–24, Cocoa Beach, FL, USA, Feb.–Mar. 2016.
20. Villanen, J., J. Ollikainen, O. Kivekäs, and P. Vainikainen, "Coupling element based mobile terminal antenna structures," *IEEE Trans. Antennas Propag.*, Vol. 54, No. 7, 2142–2153, Jul. 2006.
21. Valkonen, R., M. Kaltiokallio, and C. Icheln, "Capacitive coupling element antennas for multi-standard mobile handsets," *IEEE Trans. Antennas Propag.*, Vol. 61, No. 5, 2783–2791, Feb. 2013.
22. CST MICROWAVE STUDIO®, "3D electromagnetic simulation software," CST Computer Simulation Technology AG, Darmstadt, Germany, Online Available: https://www.cst.com/products/cstmws/.
23. Optenni Lab., "Matching circuit generation and antenna analysis software," Optenni Ltd., Espoo, Finland, Online Available: http://www.optenni.com/.
24. Rasilainen, K., A. Lehtovuori, and V. Viikari, "LTE handset antenna with closely-located radiators, low-band MIMO, and high efficiency," *Proc. 11th Eur. Conf. Antennas Propag. (EuCAP)*, 3074–3078, Paris, France, Mar. 2017.
25. Bao, Z., Z. Nie, and X. Zong, "A novel broadband dual-polarization antenna utilizing strong mutual coupling," *IEEE Trans. Antennas Propag.*, Vol. 62, No. 1, 450–454, Jan. 2014.
26. Peng, C. M., I. F. Chen, C. C. Hung, S. M. Shen, C. T. Chien, and C. C. Tseng, "Bandwidth enhancement of internal antenna by using reactive loading for penta-band mobile handset application," *IEEE Trans. Antennas Propag.*, Vol. 59, No. 5, 1728–1733, Mar. 2011.
27. Zhao, L. and K. L. Wu, "A decoupling technique for four-element symmetric arrays with reactively loaded dummy elements," *IEEE Trans. Antennas Propag.*, Vol. 62, No. 8, 4416–4421, Jun. 2014.
28. Ilvonen, J., R. Valkonen, J. Holopainen, and V. Viikari, "Design strategy for 4G handset antennas and a multiband hybrid antenna," *IEEE Trans. Antennas Propag.*, Vol. 62, No. 4, 1918–1927, Jan. 2014.
29. Zhai, G., Z. N. Chen, and X. Qing, "Enhanced isolation of a closely spaced four-element MIMO antenna system using metamaterial mushroom," *IEEE Tran. Antennas Propag.*, Vol. 63, No. 8, 3362–3370, Aug. 2015.
30. Thummaluru, S. R. and R. K. Chaudhary, "Mu-negative metamaterial filter-based isolation technique for MIMO antennas," *Electronics Lett.*, Vol. 53, No. 10, 644–646, May 2017.
31. Premix, "PREPERM® L335 datasheet," Premix Oy, Rajamäki, Finland, Online Available: http://www.premixgroup.com/wp-content/uploads/2015/02/preperm_l335_tds.pdf.
32. Blanch, S., J. Romeu, and I. Corbella, "Exact representation of antenna system diversity performance from input parameter description," *Electronics Lett.*, Vol. 39, No. 9, 705–707, May 2003.